Physically Cross-Linked Networks of POSS-Capped Poly(Acrylate Amide)s: Synthesis, Morphologies, and Shape Memory Behavior

Yuqin Cao, Sen Xu, Lei Li, Sixun Zheng

Department of Polymer Science and Engineering and State Key Laboratory of Metal Matrix Composites, Shanghai Jiao Tong University, Shanghai 200240, People's Republic of China
Correspondence to: S. Zheng (E-mail: szheng@sjtu.edu.cn)

Received 24 October 2016; accepted 21 December 2016; published online 24 January 2017
DOI: 10.1002/polb.24303

ABSTRACT: In this work, we synthesized a novel organic–inorganic semitelechelic polymer from polyhedral oligomeric silsesquioxane (POSS) and poly(acrylate amide) (PAA) *via* reversible addition-fragmentation chain transfer (RAFT) polymerization. The organic–inorganic semitelechelic polymers have been characterized by means of nuclear magnetic resonance spectroscopy, thermal gravimetric analysis, and dynamic mechanical thermal analysis. It was found that capping POSS groups to the single ends of PAA chains caused a series of significant changes in the morphologies and thermomechanical properties of the polymer. The organic–inorganic semitelechelics were microphase-separated; the POSS microdomains were formed *via* the POSS–POSS interactions. In a selective solvent (e.g., methanol), the organic–inorganic semitelechelics can be self-assembled into the micelle-like nanoobjects. Compared to plain PAA, the POSS-capped PAAs significantly displayed improved surface hydrophobicity as evidenced by the measurements of static contact angles and surface atomic force microscopy. More importantly, the organic–inorganic semitelechelics displayed typical shape memory properties, which was in marked contrast to plain PAA. The shape memory behavior is attributable to the formation of the physically cross-linked networks from the combination of the POSS–POSS interactions with the intermolecular hydrogen-bonding interactions in the organic–inorganic semitelechelics. © 2017 Wiley Periodicals, Inc. J. Polym. Sci., Part B: Polym. Phys. **2017**, *55*, 587–600

KEYWORDS: poly(acrylate amide); POSS; POSS–POSS interactions; shape memory polymers

INTRODUCTION Polyhedral oligomeric silsesquioxanes (POSS) are a class of cage-like organic–inorganic assemblies[1,2] and they generally have cube-octameric structures represented by the formula of $R_8Si_8O_{12}$. Owing to their nanometer sizes ($\sim$ 0.53 nm in diameter), POSS have been used as a class of important building blocks to access the organic–inorganic nanocomposites. It has been realized that incorporation of POSS into organic polymers can afford the materials with improved and even new thermomechanical properties.[3–8] Recently, POSS have also been employed to modulate the functional properties of some polymers *via* the formation of specific morphologies.[8–27] For instance, POSS have been incorporated into polyfluorene, polyphenylene, and polythiophene to improve their conductive and luminescent properties by controlling the stacking of the macromolecular chains.[8,9] Poly(*N*-isopropylacrylamide) hydrogels containing POSS can display accelerated thermoresponsive properties *via* the formation of hydrophobic POSS microdomains.[12–14] Shape memory polymers have attracted considerable interest and they can be used as the substitutes or competing materials for traditional shape memory alloys owing to their lightness, simplicity in processing, high shape recovery, and low cost.[29–33] Mather et al. reported that inclusion of POSS can improve the shape memory properties of organic polymers.[34–38]

Owing to the inherent immiscibility and the chemical linkages between polymers and the inorganic components, POSS-containing nanocomposites are generally microphase-separated, that is, POSS cages would be segregated from organic polymer matrix in the form of the microdomains *via* POSS–POSS interactions.[27,28] It is the formation of the POSS microdomains that endows the organic–inorganic composites with improved thermomechanical properties. Depending on the functionality of POSS macromers, POSS cages can be introduced into polymers in the forms of side groups, cross-linking sites, main-chain structural units, and end groups in organic polymers.[1–5] These organic–inorganic macromolecular architectures can significantly affect the microphase separation behavior of the composite systems. It is critical to investigate the effect of the composite architectures on the morphologies and thermomechanical properties of the materials. Nonetheless, such an investigation has long remained

unexplored although composite architecture is a key factor. Telechelics are a class of polymers (or oligomers), the ends of which are capped with reactive or functional groups[39–41]; semitelechelics have the single functionalized ends of chains. Depending on types of terminal groups, telechelics have been employed to synthesize multiblock copolymers (e.g., polyurethane) or to modify thermosets. For instance, polydiols have been used as the chain extenders to obtain multiblock polyurethanes,[42,43] whereas carboxyl (or amino)-terminated poly(butadiene-*co*-acrylonitrile)s have been used as the modifiers to improve the fracture toughness of epoxy thermosets.[44] If POSS cages are capped to the ends of polymer chains, the as-obtained organic–inorganic telechelics would display some interesting morphologies and thermomechanical properties. This class of organic–inorganic telechelics are of interest due to their specific topologies and self-assembly behavior.[13,22,45–50] Mather et al.[45] first reported the synthesis of POSS-capped poly(ethylene oxide) telechelics *via* the reaction of 3-isocyanatopropyldimethylsilylheptacyclohexyl POSS with poly (ethylene glycol); they found that the organic–inorganic telechelics exhibited surface activity at the air/water interface. Mueller et al.[48] reported the synthesis of POSS-capped polystyrene telechelics *via* the combination of atom transfer radical polymerization (ATRP) and the copper-catalyzed Huisgen 1,3-cycloaddition. More recently, Zheng et al.[50] reported the synthesis of POSS-capped PNIPAAm telechelics *via* reversible addition-fragmentation chain transfer (RAFT) polymerization approach. Owing to the highly hydrophobicity of the POSS end groups, the organic–inorganic telechelics can form the physical hydrogels. Compared to the traditional chemical hydrogels, the physical hydrogels of PNIPAAm exhibited rapid deswelling and reswelling properties.

Poly(acrylate amide) (PAA) is a novel self-associating polymer with strong intermolecular hydrogen-bonding interactions. Recently, Guan et al.[51–53] reported the synthesis of a series of the PAA copolymers with various macromolecular architectures; they found that these copolymers can display the self-healing properties *via* the synergism of the intermolecular hydrogen-bonding interactions and microphase-separated morphologies. In this work, we explored to cap POSS groups to single ends of PAA chains to afford a novel semitelechelics. The organic–inorganic semitelechelics would be microphase-separated *via* the formation of the POSS microdomains *via* POSS–POSS interactions. It is expected that the combination of the POSS microdomains with the self-association *via* the intermolecular hydrogen-bonding interactions would result in the formation of physically cross-linked networks. The purpose of this work is twofold: (i) to investigate the formation of the POSS microdomains and (ii) to examine the effect of the POSS microdomain formation on the thermomechanical properties such as surface hydrophobicity and shape memory behavior. Toward this end, the morphologies of the organic–inorganic semitelechelics were investigated by means of transmission electron microscopy (TEM), small-angle X-ray scattering (SAXS), and dynamic laser scattering (DLS). The surface properties were investigated with the measurements of static contact angles and surface atomic force microscopy (AFM). The shape memory properties of the organic–inorganic semitelechelics were addressed on the basis of the creep-recovery tests.

EXPERIMENTAL

Materials

Phenyltrimethoxysilane (98%) was supplied by Zhejiang Chemical Technology Co., China and it was distilled under reduced pressure before use. Trichlorosilane and trimethylchlorosilane were purchased from Sigma Aldrich Co., China and used as received. Sodium hydroxide and acetic anhydride were obtained from Shanghai Reagent Co., China. 2,2-Azobisisobutylnitrile (AIBN) was used as the initiator; it was recrystallized from ethanol twice. Both 1-(3-Dimethylaminopropyl)-3-ethylcarbodiimide hydrochloride and 4-dimethylaminopyridine were of chemically pure grade, purchased from Admas Reagent Co., Shanghai, China. 2-Methyl-2-[(dodecylsulfanylthiocarbonyl) sulfanyl]propanoic acid was synthesized as described by McCormick et al.[54]; 5-acetamidopenpental acrylate was prepared by following the method of literature.[51] The organic solvents such as toluene, tetrahydrofuran (THF), methanol, *N*,*N*-dimethylformamide (DMF), and chloroform were of chemically pure grade, obtained from commercial sources. Before use, toluene and THF were refluxed above metal sodium and then distilled; DMF was distilled over calcium hydride (CaH_2) under decreased pressure.

Synthesis of Hydroheptaphenyl POSS

First, heptaphenyltricycloheptasiloxane trisodium silanolate [$Na_3O_{12}Si_7(C_6H_5)_7$] was synthesized by following the method of literature.[55] To a flask equipped with a condenser and a magnetic stirrer, phenyltrimethoxysilane [$C_6H_5Si(OMe)_3$] (49.500 g, 0.25 mol), THF (250 mL), deionized water (5.670 g, 0.32 mol), and sodium hydroxide (4.350 g, 0.1 mol) were added with vigorous stirring. After refluxing for 5 h, the system was cooled down to room temperature, at which the reaction was performed for additional 15 h. After that, all the solvents and other volatile components were removed *via* rotary evaporation. After drying *in vacuo* at 50 °C for 24 h, the product [i.e., $Na_3O_{12}Si_7(C_6H_5)_7$] (34.800 g) was obtained with the yield of 98%.

Second, the silylation reaction of $Na_3O_{12}Si_7(C_6H_5)_7$ with trichlorosilane was carried out to afford hydroheptaphenyl POSS (denoted POSS-H). Typically, $Na_3O_{12}Si_7(C_6H_5)_7$ (34.800 g, 34.9 mmol) was added to a flask and then anhydrous THF (250 mL) was added with vigorous stirring. The flask was immersed into an ice-water bath and purged with highly pure nitrogen for 1.5 h. Thereafter, trichlorosilane (5.260 g, 34.8 mmol) was added and the reaction was performed at 0 °C for 4 h and at room temperature for 24 h. The insoluble component (i.e., sodium chloride) was filtered out and the solvent together with other volatile compounds was removed *via* rotary evaporation. The solids were washed with 200 mL of methanol three times and dried *in vacuo* at 30 °C for 24 h. The product (19.700 g) was obtained with the yield of 59.6%. ^{1}H NMR (ppm, $CDCl_3$): 7.30–7.55, 7.70–7.87 (35H, $C_6\boldsymbol{H}_5$–), and 4.50 (*s*, Si***H***).

Synthesis of 3-Hydroxylpropylheptaphenyl POSS

First, 3-trimethylsilylheptaphenyl POSS was synthesized *via* the hydrosilylation reaction of POSS-H with allyloxytrimethylsilane. POSS-H (8.000 g, 8.36 mmol), allyloxytrimethylsilane (5.400 g,

41.54 mmol), and anhydrous toluene (80 mL) were added to a flask containing a magnetic stirrer. The flask was connected to a Schlenk line to degas with a repeated exhausting-refilling process with highly pure nitrogen and then Karstedt catalyst was added with vigorous stirring. The reaction was performed at 95 °C for 36 h to attain a complete reaction. The toluene and excess allyloxytrimethylsilane were removed *via* rotary evaporation and the product (8.200 g) was obtained with the yield of 90%.

Second, 3-hydroxylpropylheptaphenyl POSS was prepared *via* the deprotection reaction of 3-trimethylsilylpropylheptaphenyl POSS. The above 3-trimethylsilylpropyl heptaphenyl POSS (3.000 g, 2.76 mmol) was dissolved in 90 mL of dichloromethane and then 90 mL of methanol was added with vigorous stirring. The reaction was performed at room temperature for 5 h. Thereafter, methyltrichlorosilane (0.680 g, 6.26 mmol) was dropwise added within 30 min with vigorous stirring. The solvent and excess methyltrichlorosilane were removed *via* rotary evaporation. The resulting product (1.800 g) was obtained *via* a recrystallization from the mixture of THF and hexane (50/50 vol) with the yield of 60%. ^{1}H NMR (ppm, $CDCl_3$): 7.30–7.55, 7.70–7.87 (35H, $C_6\boldsymbol{H}_5$—), 3.61 (*t*, 2H, —$CH_2CH_2C\boldsymbol{H}_2OH$), 1.78 (*m*, 2H, —$CH_2C\boldsymbol{H}_2CH_2OH$), 0.90 (*t*, 2H, —$C\boldsymbol{H}_2CH_2CH_2OH$).

Synthesis of POSS-CTA

3-Hydroxylpropylheptaphenyl POSS (7.000 g, 6.9 mmol) and 2-methyl-2-[(dodecylsulfanylthiocarbonyl)sulfanyl]propanoic acid (7.540 g, 20.71 mmol) dissolved in 10 mL of anhydrous CH_2Cl_2 were added to a flask equipped with a magnetic stirrer. 1-(3-Dimethylaminopropyl)-3-ethylcarbodiimide hydrochloride (3.310 g, 17.26 mmol) and 4-dimethylaminopyridine (0.080 g, 65.57 mmol) were then added. The reaction was performed at room temperature for 24 h; the reacted mixture was concentrated *via* rotary evaporation and then dropped into 100 mL of methanol to afford the precipitates (viz. the POSS-CTA). After drying *in vacuo* at 40 °C or 12 h, the product (8.700 g) was obtained with the yield of 90%. ^{1}H NMR (ppm, $CDCl_3$): 7.30–7.55 (35H, $C_6\boldsymbol{H}_5$—), 4.10 [*t*, 2H, —$CH_2CH_2C\boldsymbol{H}_2COO$—], 3.16 [*t*, 2H, —$CSCSSC\boldsymbol{H}_2(CH_2CH_2)_5$–], 1.92 [*m*, 2H, —$C\boldsymbol{H}_2CH_2CH_2COO$—], 1.70 [*m*, 6H, —$COOC(C\boldsymbol{H}_3)_2SCSS$—], 1.25 [*m*, 20H, —$CH_2(C\boldsymbol{H}_2C\boldsymbol{H}_2)_5CH_3$] and 0.92 [*m*, 5H, $(CH_2)_2C\boldsymbol{H}_2COOC(CH_3)_2$ $SCSSCH_2(CH_2CH_2)_5C\boldsymbol{H}_3$].

Synthesis of POSS-Capped PAAs

Typically, POSS-CTA (1.630 g, 1.57 mmol), 5-acetamidopenpental acrylate (6.000 g, 30 mmol), and *N,N*-dimethylformamide (10 mL) were added to a flask with vigorous stirring. Thereafter, AIBN (39.36 mg, 0.24 mmol) was added and the system was purged with highly pure nitrogen for 30 min. The polymerization was carried out at 60 °C for 24 h; the polymerized mixture was dropped into 100 mL of anhydrous diethyl ether to afford the precipitates. After drying *in vacuo* at 100 °C for 24 h, the polymer (viz. POSS-capped PAA) (6.190 g) was obtained with the conversion of AA to be 85%. ^{1}H NMR (ppm, DMSO-d_6): 7.82 (*s*, —$CH_2N\boldsymbol{H}COCH_3$), 3.98 (*t*, 2H, —$COOC\boldsymbol{H}_2CH_2$—), 3.35 (*m*, –$CCH_2C\boldsymbol{H}COO$—), 3.01 (*m*, 2H, —$CH_2C\boldsymbol{H}_2NH$—), 1.98 (*m*, –$NHCOC\boldsymbol{H}_3$), 1.80 (*m*, —$CC\boldsymbol{H}_2CHCOO$—), 1.54 (*t*, —$COOCH_2C\boldsymbol{H}_2CH_2CH_2CH_2$—), 1.37 (*t*, —$COOCH_2CH_2CH_2C\boldsymbol{H}_2CH_2$—), and 1.28 (*t*, —$COOCH_2CH_2C\boldsymbol{H}_2CH_2CH_2$—).

Measurements and Techniques

Nuclear Magnetic Resonance (NMR) Spectroscopy

The ^{1}H NMR spectroscopy was carried out on a Varian Mercury Plus 400 MHz NMR spectrometer at 25 °C. The samples were dissolved in deuterium chloroform ($CDCl_3$) or dimethylsulfoxide (DMSO-d_6). The solutions were measured with tetramethylsilane (TMS) as an internal reference.

Thermal Gravimetric Analysis (TGA)

The TGA measurements were carried out on a TA Q-5000 thermogravimetric analyzer. In air atmosphere, the samples (about 10.0 mg) were heated from room temperature to 800 °C at the heating rate of 20 °C × min^{-1}.

Transmission Electron Microscopy (TEM)

The morphological observations were performed on a JEOL JEM-2010 TEM at an acceleration voltage of 120 kV. To investigate the microphase-separated morphologies, all the POSS-capped PAAs were dissolved in DMF at the concentration of 2.0 g L^{-1}; the solutions were dropped onto 200-mesh copper grids and the solvent was evaporated at 40 °C overnight and the residual solvent was removed in a vacuum oven at 40 °C for 48 h. To investigate the self-assembly behavior of POSS-capped PAAs in methanol, the specimens were prepared by dropping the suspensions of the polymers in methanol (about 10 μL at 0.2 g L^{-1}) onto copper grids and the solvent was evaporated *via* a freeze-drying approach.

Dynamic Light Scattering (DLS)

The POSS-capped PAAs (10.0 mg) were dissolved in 1 mL of DMF and the solutions were dropwise added to 100 mL of methanol. The DMF solvent was eliminated with dialysis in methanol. The suspensions were then subjected to DLS on a Malvern Nano ZS90 apparatus equipped with a He–Ne laser operated at the wavelength of $\lambda = 633$ nm. In the DLS measurements, the data were collected at a fixed scattering angle of 90°.

Dynamic Mechanical Thermal Analysis (DMTA)

The rectangular specimens were prepared *via* solution-casting approach with DMF as the solvent. The solvent was eliminated *in vacuo* at 60 °C for at least 2 weeks. The DMTA measurements were carried out on a TA DMA Q-800 apparatus with a tensile mode with the frequency of 1 Hz. To measure the glass transition temperatures and moduli, the specimens with the dimension of 20 × 5 × 2 mm^3 were heated from −40 °C at the heating rate of 3 °C min^{-1} until the specimens became too soft to be tested. The creep tests were carried out with the constant stress of σ = 100 N m^2 within 1 h and the recovery tests were performed within 4 h.

Atomic Force Microscopy (AFM)

The surface morphologies of the POSS-capped PAA films were investigated by means of AFM with a tapping mode. First, the solutions of the POSS-capped PAAs dissolved in DMF at the concentration of 10 wt % were spin-coated onto the silicon wafers. The solvent was removed at 60 °C

overnight. The residual solvent was eliminated *in vacuo* at 40 °C for 48 h. The films of the samples with the thickness of about 25 μm were used for the surface morphological observation. The AFM experiments were performed on a CSPM 5500 AFM (Benyuan Nano-instruments Ltd, China). The tips fabricated from silicon (125 μm in length with ca 500 kHz resonant frequency) were used and the scanning rate was 2.0 Hz in tapping mode. Typical scan speeds was 0.3–1 lines $\times$ s^{-1} with a maximum range of 10 $\times$ 10 μm.

Contact Angle Measurements

The above specimens of films were also used for the measurement of contact angle. The static contact angle measurements were carried out on a DSA30 contact angle measurement instrument (Krüss GmbH, Germany) at room temperature and ultrapure water and diiodomethane were used as probe liquids, respectively. The values of contact angles were taken from the average of three parallel measurements.

Shape Memory Analysis

To investigate the shape memory properties of the POSS-capped PAAs, the samples were prepared into the rectangular specimens with the dimensions of 60 $\times$ 2 $\times$ 2 mm^3. Before the measurement, the samples were stored at 60 °C for 12 h to erase the thermal history and then the samples were deformed into "C" shape at this temperature (Scheme 1). Thereafter, the deformed samples were rapidly quenched to −20 °C in a refrigerator and maintained at that temperature for 12 h; the bent samples were taken out and placed in the thermal stage maintained at 25 °C. The shape recovery process was pictured with a digital camera.

The shape memory behavior was also investigated with one-way measurements of dynamic mechanical thermal analysis (DMTA) on the TA DMA Q800 apparatus. This measurement began at 35 °C with the following four programs: (i) deformation: a rectangular POSS-PAA2K specimen was elongated by increasing the applied load from 0 to 0.11 N at a rate of 0.03 N min^{-1} at 35 °C; (ii) fixing: the specimen was then cooled at 3 °C min^{-1} to −40 °C under constant load to fix the temporary shape; (iii) unloading: the load was removed at a constant rate of 0.03 N min^{-1} revealing the quality of fixing through the resulting final strain; and (iv) recovery: a heat-induced recovery toward the original length was examined by heating to 35 °C at a rate of 3 °C min^{-1}.

RESULTS AND DISCUSSION

Synthesis of POSS-Capped PAAs

The route of synthesis for POSS-capped PAAs is shown in Scheme 2. First, 3-hydroxylpropylheptaphenyl POSS was synthesized; it was then employed to react with 2-methyl-2-[(dodecylsulfanylthiocarbonyl) sulfanyl]propanoic acid to afford a chain transfer agent (denoted POSS-CTA). Thereafter, the radical polymerization of 5-acetamidopenpental acrylate (AA) was carried out, which was mediated with the POSS-CTA to afford a series of POSS-capped PAAs with variable lengths of PAA (Table 1). In this work, 3-hydroxylpropylheptaphenyl POSS was synthesized with the combination of silylation and hydrosilylation reactions. The silylation reaction was carried out between heptaphenyltricycloheptasiloxane trisodium silanolate [$Na_3O_{12}Si_7(C_6H_5)_7$] and trichlorosilane to afford hydroheptaphenyl POSS (denoted POSS-H). Herewith, $Na_3O_{12}Si_7(C_6H_5)_7$ was prepared *via* the hydrolysis, condensation, and rearrangement of phenyltrimethoxysilane in the presence of sodium hydroxide (NaOH) by following the method reported by Koh et al.[55] The hydrosilylation reaction between POSS-H and allyloxytrimethylsilane afforded 3-trimethylsilylpropylheptaphenyl POSS. The latter was deprotected to obtain 3-hydroxylpropylheptapehnyl POSS [viz. $POSS(CH_2)_3OH$]. The POSS-CTA was obtained *via* the esterification reaction of $POSS(CH_2)_3OH$ with 2-methyl-2-[(dodecylsulfanylthiocarbonyl)-sulfanyl]propanoic acid. Shown in Figure 1 are the ^1H NMR spectra of $POSS(CH_2)_3OH$, POSS-CTA, and POSS-capped PAA2K. For $POSS(CH_2)_3OH$, the signals of resonance at 0.90, 1.78, and 3.61 ppm are assignable to the protons of three methylene groups in 3-hydroxypropyl group as indicated. Compared to $POSS(CH_2)_3OH$, several new signals of resonance appeared at 0.92, 1.25, 1.70, 1.92, 3.16, and 4.10 ppm in the ^1H NMR spectrum of POSS-CTA; they are assignable to the protons of methylene and methyl groups in the moiety of trithioester (i.e., the chain transfer agent, CTA). Notably, the signal of resonance at 3.61 ppm, assignable to the methylene protons of hydroxymethyl group in $POSS(CH_2)_3OH$ was observed to shift to 4.10 ppm owing to the occurrence of the esterification reaction. For POSS-capped PAA, the signals of resonance resulting from the protons of PAA were detected at 1.28, 1.37, 1.54, 1.80, 1.98, 3.01, 3.35, and 3.98 ppm, which are assignable to the protons of methylene, methine, and methyl groups as indicated in Figure 1. The signal of resonance assignable to the proton of N—H in amide group was detected at 7.82 ppm. In addition, the resonance of phenyl protons from POSS cages was discernible in the range of 7.06–7.73 ppm. The ^1H NMR spectroscopy indicates that $POSS(CH_2)_3OH$ and POSS-CTA have been successfully obtained. The polymerized product combined the structural features from PAA and POSS. In this work, the POSS-capped PAAs with various lengths of PAA chains were synthesized by controlling the molar ratios of POSS-CTA to AA. Unfortunately, we failed to measure the molecular weights of the POSS-capped PAAs by means of gel permeation chromatography (GPC) as the commonly used single-component GPC eluents such as THF, DMF, and chloroform were not the cosolvents of the organic (viz. PAA) and the inorganic (i.e., POSS) portions of the organic–inorganic semitelechelics. Herewith, we estimated the length of PAA chains according to the ratios of the integral intensity of the resonance at 0.92 ppm assignable to the protons of the methylene connected to silicon atom to those of PAA chains (e.g., at 1.79 ppm) in the ^1H NMR spectra of POSS-PAAs. Alternatively, we utilized the TGA measurements to estimate the lengths of PAA chains according to the end group analysis. Shown in Figure 2 are the TGA curves of POSS-CTA and the POSS-capped PAAs in air atmosphere. Under this condition, notably, a plain PAA (M_n = 20,000 Da with M_w/M_n = 1.10) was almost completely decomposed at 800 °C. In contrast, all the POSS-capped PAAs exhibited the residues of degradation, the yields of which increased with decreasing the lengths of PAA

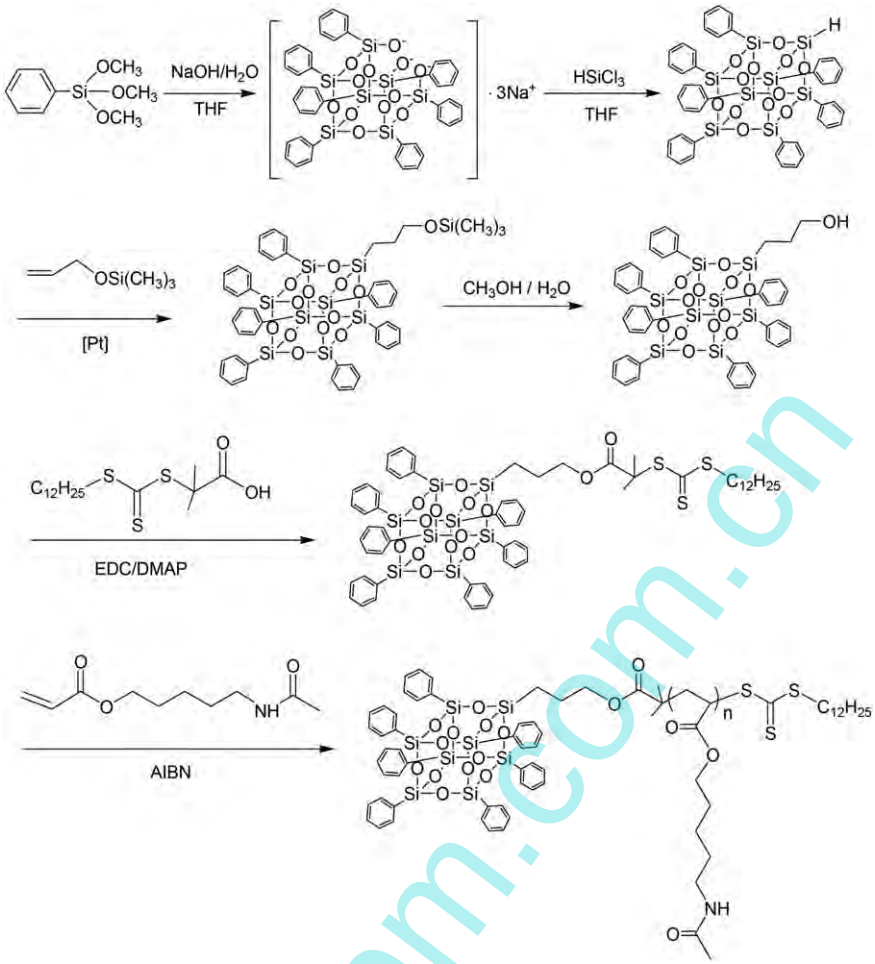

SCHEME 1 Synthesis of POSS-capped poly(acrylate amide).

chains. Assuming that the residues of degradation were from the decomposition and oxidation of POSS cages, the lengths of PAA chains were thus calculated according to the yields of degradation residues at 800 °C. The lengths of PAA chains in the POSS-capped PAAs are summarized in Table 1.

Morphologies and Dynamic Mechanical Properties

All the POSS-capped PAAs were subjected to TEM measurements to investigate the morphologies; the TEM micrographs are shown in Figure 3. It is seen that all the POSS-capped PAAs were microphase-separated. The spherical or worm-like microdomains with the size of 20–100 nm in diameter were dispersed in the continuous matrices; the microdomain sizes decreased with increasing the lengths of PAA chains. According to the contents of POSS in the POSS-capped PAAs and the difference in electron density between POSS and PAA, it is judged that the dark microdomains are attributable to the POSS aggregates *via* POSS–POSS interactions, whereas the light regions to PAA matrix. The microphase-separated morphologies were further confirmed by SAXS as shown in Figure 4. In all the cases, the POSS-capped PAAs displayed the intense scattering peaks with the values of scattering vectors (q) in the range of 0.5–0.6 nm^{-1}; the scattering peaks gradually shifted to the positions with low q values with increasing the lengths of PAAs. The appearance of the scattering peaks indicates that the POSS-capped PAAs were indeed microphase-separated. According to the position of the scattering peaks, the long periods (L) in the samples were calculated with Bragg equation ($L = 2\pi/q$). It is seen that the long periods (viz. the average distance among the adjacent POSS microdomains) increased with increasing the lengths of PAA chains. The results of SAXS were in good agreement with those of TEM.

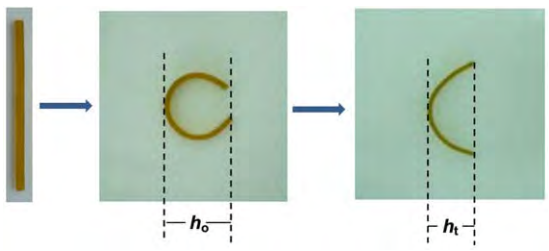

SCHEME 2 Preparation of the specimens for shape-memory experiments. [Color figure can be viewed at wileyonlinelibrary.com]

TABLE 1 The Molecular Weights of POSS-Capped PAA Copolymers

Samples	M_n (Da)*	L_{PAA} (Da)	POSS (wt %)[a]	POSS (wt %) at Surface[b]
PAA	20,000	20,000	–	–
POSS-PAA2K	3100	2150	30.8	59
POSS-PAA4K	4500	3550	21.2	54
POSS-PAA5K	5700	4750	17.0	45
POSS-PAA7K	8000	7050	11.9	41

[a] The values were calculated on the basis of the yields of degradation in air atmosphere at 800 °C.
[b] The values were estimated on the basis of the AFM results (Fig. 9) by using ImageJ software [59].

Shown in Figure 5 are the DMTA curves of the POSS-capped PAAs. In the experimental range of temperature, single peaks were exhibited in all the cases. The single peaks are attributable to the glass transitions of PAA matrices; the T_gs increased with increasing the lengths of PAA chains. It is proposed that following two opposite factors could affect the glass transition temperatures (T_gs) of the POSS-capped PAAs. On one hand, the T_gs increased with increasing the lengths of PAA chains. The variation of T_g with molecular weights can be well interpreted on the basis of the changes of free volume fraction as a function of quantity of free ends of PAA chains. The higher the percentage of free volume, the shorter the PAA chains (i.e., the smaller the molecular weights of PAAs). On the other hand, the

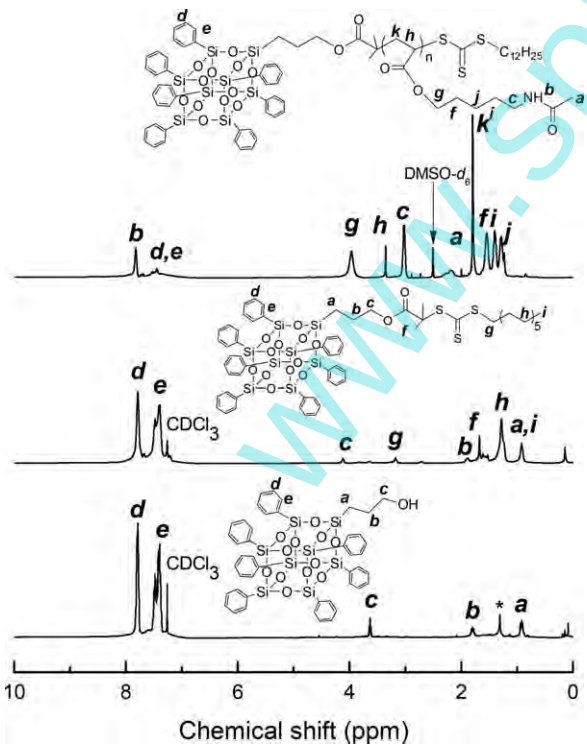

FIGURE 1 ^{1}H NMR spectra of POSS-PAA2K, POSS-CTA, and 3-hydroxylheptaphenyl POSS. The asterisk resonance resulted from a trace of water in $CDCl_3$.

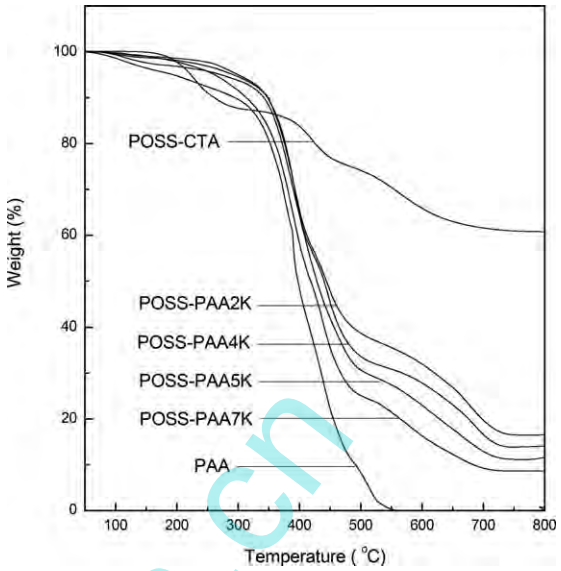

FIGURE 2 TGA curves of POSS-CTA and POSS-PAA2K, POSS-PAA4K, POSS-PAA5K, and POSS-PAA7K.

nanoreinforcement of the POSS microdomains caused the increase in T_gs owing to the restriction of the POSS microdomains on the motion of PAA segments. In the POSS-capped PAAs, the lengths of PAA chains were inversely proportional to the contents of POSS cages. Therefore, the T_gs of the POSS-capped PAAs reflected the combined contribution of the above opposite tendencies. Notably, POSS-PAA5K and POSS-PAA7K displayed the quite close T_gs, suggesting that the nanoreinforcement of POSS microdomains has counteracted the depression in T_g owing to the lower molecular weights. The T_gs of all the POSS-capped PAAs were lower than 20 °C, suggesting that the POSS-capped PAAs were in rubbery state at room temperature.

Self-Assembly Behavior in Selective Solvent

It is expected that POSS-capped PAA would display self-assembly behavior in its selective solvents. In this work, methanol was used to one of the selective solvents as the POSS was insoluble in methanol, whereas PAA was readily dissolved in methanol. The self-assembly behavior of the POSS-capped PAAs were investigated by means of TEM and DLS. In the TEM measurements, the specimens were prepared *via* freeze-drying approach with the solutions of methanol at the concentration of 2 g L^{-1} at 25 °C and the TEM images are presented in Figure 6. Notably, the spherical nano-objects were observed in all the cases. The self-assembly of all the POSS-capped PAAs in methanol generated the spherical nano-objects with the size of 20–50 nm in diameter. It is proposed that the spherical nano-objects were composed of the cores of POSS aggregates *via* POSS–POSS interactions and PAA coronas. Notably, the sizes of the spherical nano-objects decreased with increasing the lengths of PAA chains. From POSS-PAA2K to POSS-PAA7K, the size of the spherical nano-objects was decreased from 50 to 20 nm in diameter. The suspensions of the POSS-capped PAAs dispersed in methanol were subjected to dynamic light

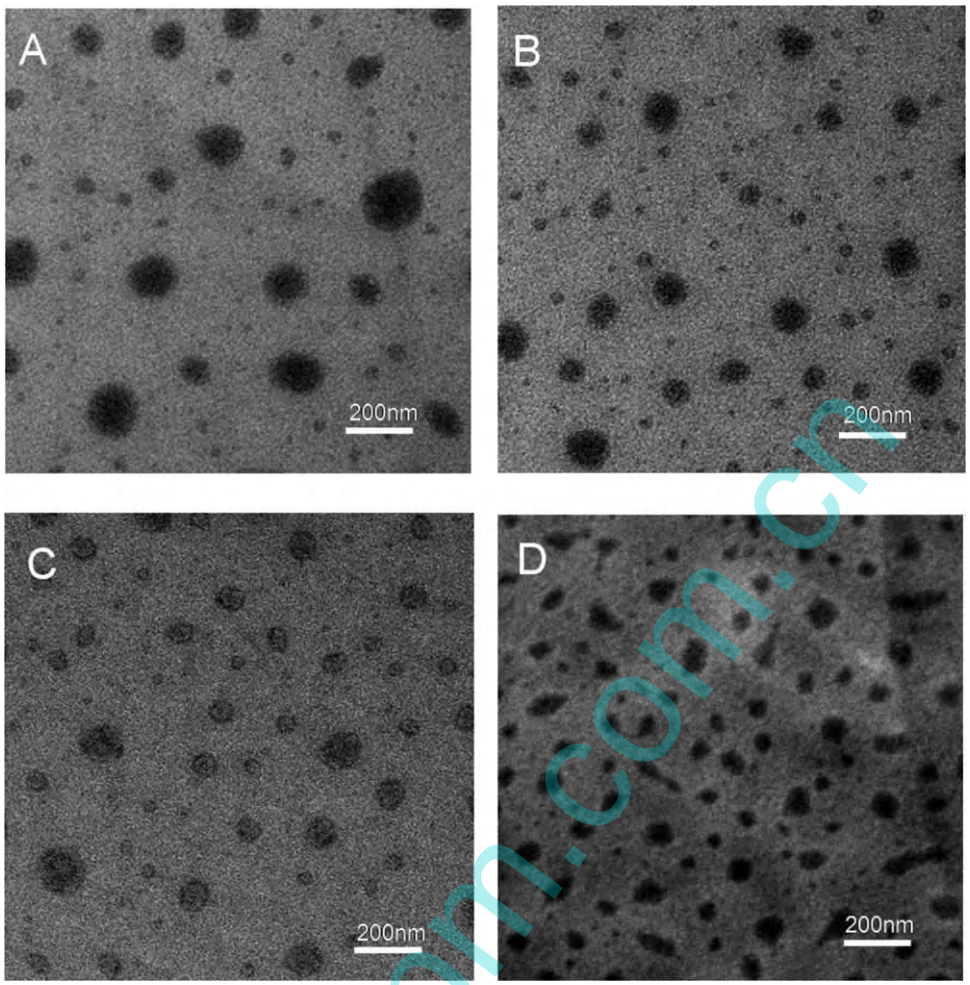

FIGURE 3 TEM images of (A) POSS-PAA2K, (B) POSS-PAA4K, (C) POSS-PAA5K, and (D) POSS-PAA7K.

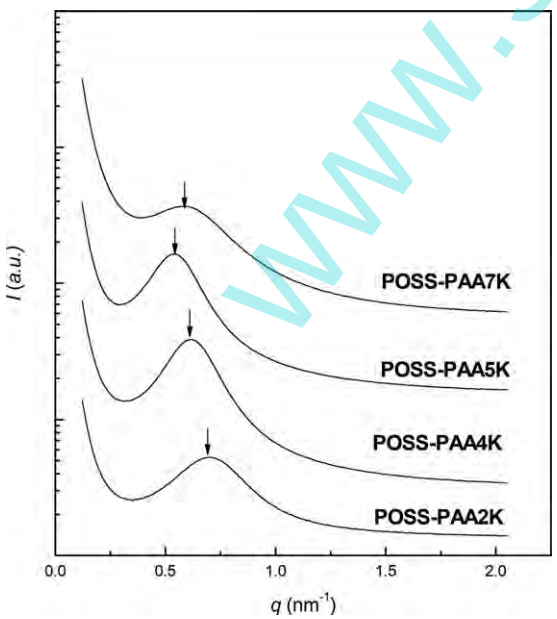

FIGURE 4 SAXS curves of POSS-PAA2K, POSS-PAA4K, POSS-PAA5K, and POSS-PAA7K.

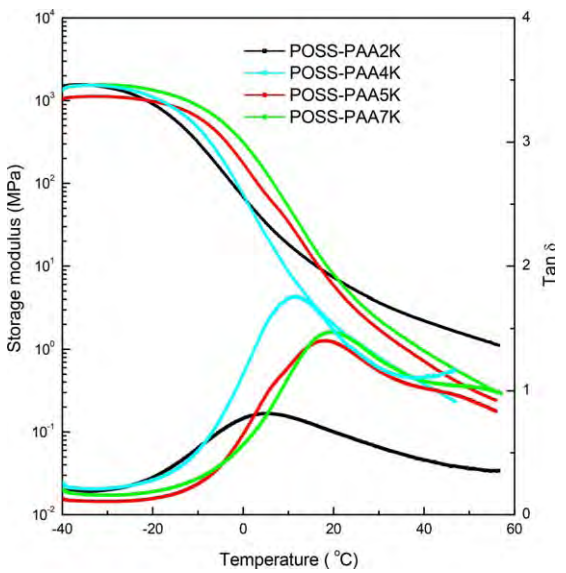

FIGURE 5 DMTA curves of POSS-PAA2K, POSS-PAA4K, POSS-PAA5K, and POSS-PAA7K. [Color figure can be viewed at wileyonlinelibrary.com]

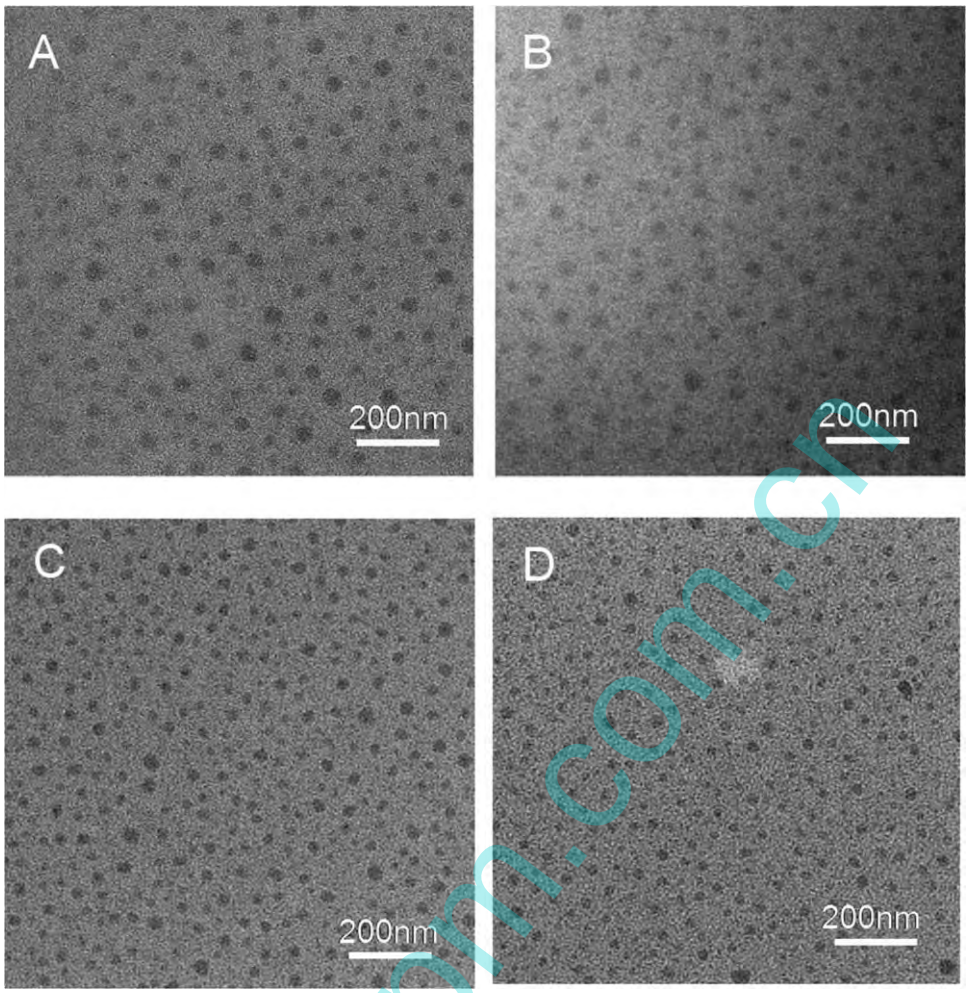

FIGURE 6 TEM images of the self-assembled nano-objects from the suspensions of (A) POSS-PAA2K, (B) POSS-PAA4K, (C) POSS-PAA5K, and (D) POSS-PAA7K dispersed in methanol at the concentration of 0.2 g L^{-1}.

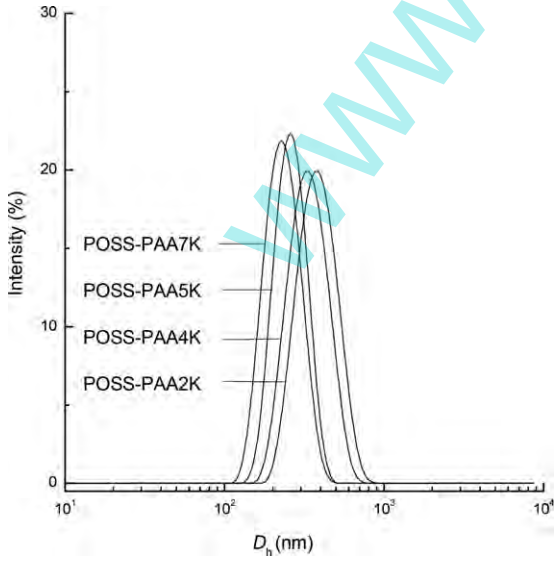

FIGURE 7 Hydrodynamic radius of POSS-capped PAAs dispersed in methanol at the concentration of 1.0 g L^{-1} at 25 °C.

scattering (DLS) to measure the hydrodynamic radii of the organic–inorganic micelle-like aggregates. Shown in Figure 7 are the plots of hydrodynamic radius distribution as functions of hydrodynamic radius (R_h) at 25 °C. In all the cases, the intensity-averaged hydrodynamic radius (R_h) displayed unimodal distribution. The R_h values were measured to be 372, 325, 259, and 227 nm for POSS-PAA2K, POSS-PAA4K, POSS-PAA5K, and POSS-PAA7K, respectively. The R_h values decreased with increasing the lengths of PAA chains. This trend was in good agreement with that observed by means of TEM. It should be pointed out that the sizes of the self-organized nano-objects measured with TEM (Fig. 6) were much lower than those values by means of DLS (Fig. 7). The difference in the value of nano-object size could result from the difference in the state of the nano-objects. The former were obtained in the dry state and were much lower than the latter obtained in the suspensions of, which contains the dominant contribution of the solvated coronas.

Enrichment Behavior of POSS onto Surfaces

The POSS cages capped at the single ends of PAA chains were the organosilicon component. Owing to the low surface

TABLE 2 Static Contact Angles and Surface Free Energy of PAA and POSS-Capped PAAs

	Static Contact Angle		Surface Free Energy (mN × m^{-1})		
Samples	Θ_{water} (°)	$\Theta_{diiodomethane}$ (°)	γ^d_s	γ^p_s	γ_s
PAA	24.6 ± 4.02	38.5 ± 0.13	26.1	40.8	66.9
POSS-PAA7K	73.6 ± 3.07	40.6 ± 0.08	33.9	7.45	41.35
POSS-PAA5K	77.3 ± 1.90	41.6 ± 0.66	34.3	5.71	40.01
POSS-PAA4K	79.3 ± 0.56	43.3 ± 0.55	33.8	5.03	38.83
POSS-PAA2K	79.8 ± 1.03	46.0 ± 0.81	32.3	5.21	37.51

free energy, the POSS cages would have the tendency to migrate onto the surface of the materials in bulks, which caused the decrease in surface free energy. This effect was readily examined with surface contact measurements. In this work, the films of plain PAA (M_n = 20,000 Da M_w/M_n = 1.10) and the POSS-capped PAAs with free surfaces were prepared *via* spin-coating approach and were used to investigate the surface hydrophobicity with surface contact angle measurements. In the measurements, ultrapure water and diiodomethane were used as the probe liquids, respectively. For the plain PAA, the water contact angle was measured to be 24.6°, a very low value, suggesting that this polymer was quite hydrophilic. Upon capping POSS cages to the single ends of chains, the water contact angles were significantly enhanced, enhancing with increasing the percentage of POSS in the POSS-capped PAAs (or decreasing with increasing the lengths of PAA chains). For POSS-PAA2K, the water contact angle was measured to be as high as 79.8°. The increased surface contact angles indicate that the surface free energy was significantly decreased. Herewith, the values of surface free energy were calculated according to the following geometric mean model[56–58]:

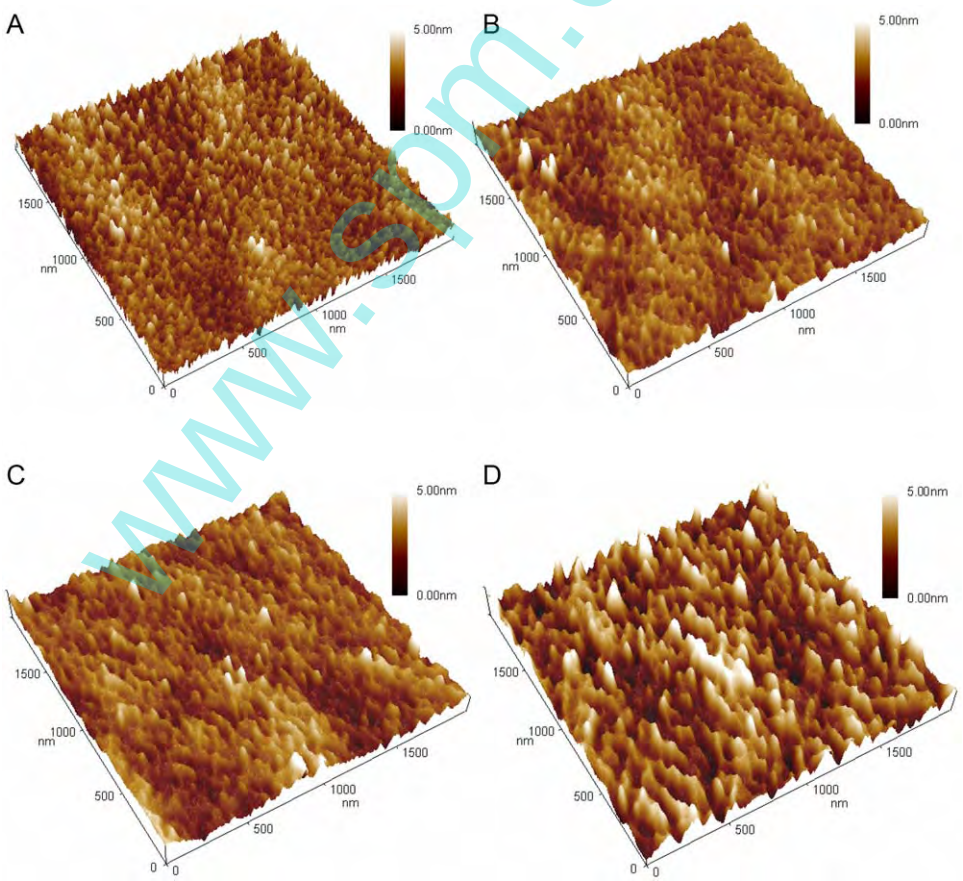

FIGURE 8 AFM height images of (A) POSS-PAA2K, (B) POSS-PAA4K, (C) POSS-PAA5K, and (D) POSS-PAA7K. [Color figure can be viewed at wileyonlinelibrary.com]

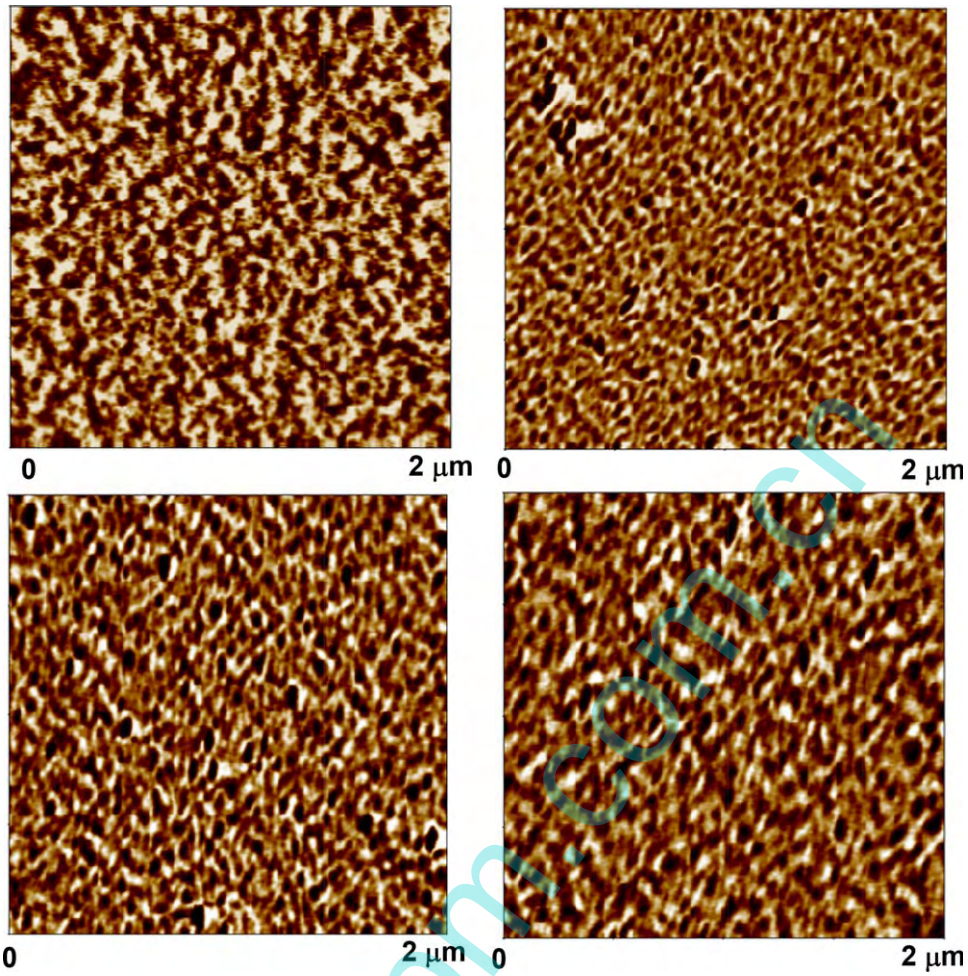

FIGURE 9 AFM phase images of (A) POSS-PAA2K, (B) POSS-PAA4K, (C) POSS-PAA5K, and (D) POSS-PAA7K. [Color figure can be viewed at wileyonlinelibrary.com]

$$\cos\theta = \frac{2}{\gamma_L}\left[(\gamma_L^d\gamma_s^d)^{\frac{1}{2}} + (\gamma_L^p\gamma_s^p)^{\frac{1}{2}}\right] - 1 \quad (1)$$

$$\gamma_s = \gamma_s^d + \gamma_s^p \quad (2)$$

where θ is the contact angle and γ_L is the liquid surface tension; γ_s^d and γ_s^p are the dispersive and polar components of γ_L, respectively. The results of contact angles and surface free energy are summarized in Table 2. For the plain PAA, the surface free energy was calculated to be 66.9 mN m^{-1}. For POSS-PAA2K, the free energy was decreased to 37.5 mN m^{-1}. Notably, the polar component (i.e., γ_s^p) was very sensitive to the percentage of POSS in the POSS-capped PAAs. This observation suggests that capping POSS cages to the chain ends of PAAs significantly changed the distribution of the polar groups at the surface energy of the materials. It is proposed that the component with the lower surface free energy (viz. POSS) was enriched onto the surfaces of the materials. The POSS cages at the surfaces would act as the screening agent to the polar groups of PAAs and thus improved the surface hydrophobicity.

To investigate the distribution of POSS cages at the surface of the POSS-capped PAAs, the surface morphologies of the film specimens were investigated by means of AFM. The AFM height and phase diagrams of the POSS-capped PAAs are shown in Figures 8 and 9, respectively. Notably, the surface roughness of the films slightly decreased with increasing the percentage of POSS in the semitelechelics. In all the case, nonetheless, the surface fluctuation was within 5 nm, implying that the surfaces were quite flat (Fig. 8). Therefore, the phase images can reflect the distribution of POSS at the surface of the specimens. It is seen that all the surfaces of the POSS-capped PAAs were microphase-separated (Fig. 9). In terms of the difference in viscoelasticity between POSS microdomains and PAAs, it is judged that the light regions are responsible for the POSS microdomains, whereas the dark for PAA microphases. The fraction of the POSS microdomains in the AFM micrographs can reflect the contents of POSS microdomains at the surfaces of the POSS-capped PAAs. In this work, the fractions of the POSS microdomains were analyzed by the use of ImageJ software[59] and the values are summarized in Table 1. Notably, the values of POSS microdomain fractions at the surface were significantly

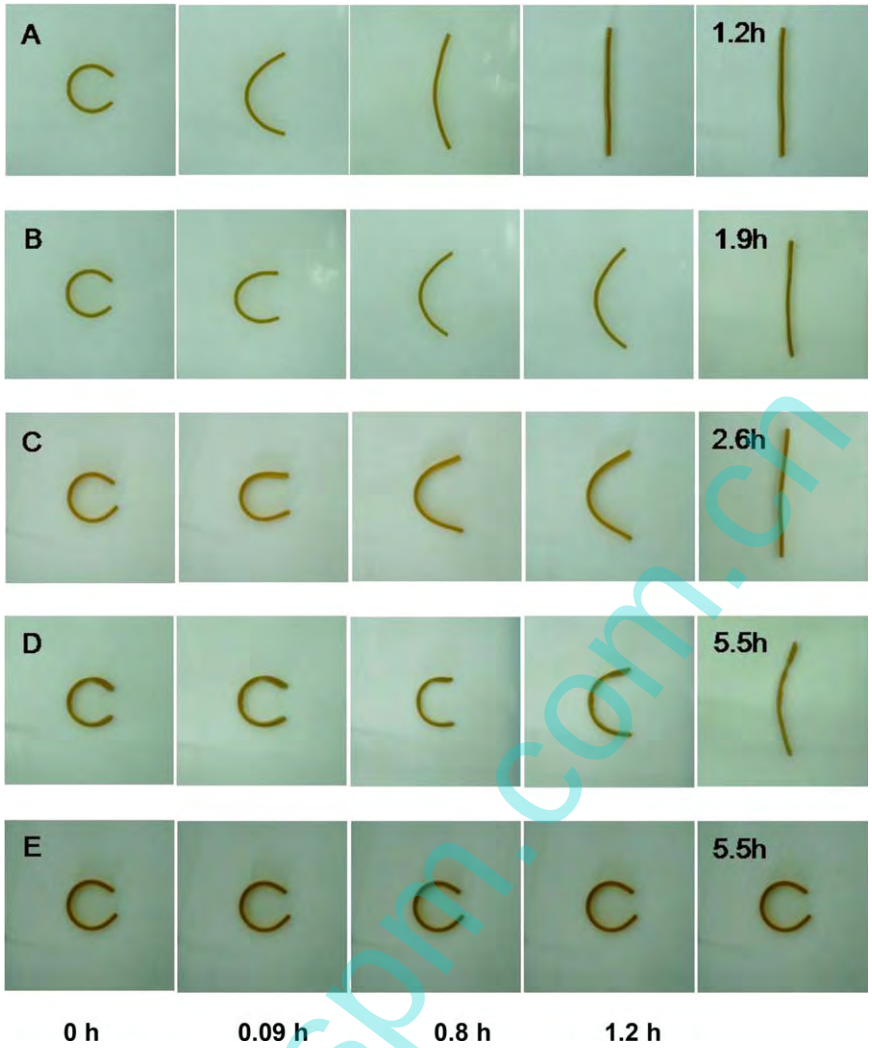

FIGURE 10 Shape recovery of (A) POSS-PAA2K, (B) POSS-PAA4K, (C) POSS-PAA5K, (D) POSS-PAA7K, and (D) Plain PAA ($M_n = 20{,}000$ Da with $M_w/M_n = 1.10$) isothermally at 25 °C. [Color figure can be viewed at wileyonlinelibrary.com]

higher than the percentages of POSS in the POSS-capped PAAs. This observation indicates that the POSS microdomains have been enriched at the surface of the materials. It is the enrichment of POSS microdomains that resulted in the decrease in surface free energy.

Shape Memory Properties

The plain PAA and POSS-capped PAAs were subjected to the shape memory experiments. Starting from the rectangular shapes at room temperature, all the specimens were deformed into the open semicircles with the fixed distances between two ends of each specimen through bending (Scheme 1). These deformed specimens were cooled to −20 °C, at which the specimens were hold for 12 h, to fix the temporary shapes completely. Thereafter, the specimens were taken out and then were isothermally held at 25 °C to observe the evolution of the specimen shapes as functions of time. It was found that except from the plain PAA, all the POSS-capped PAAs were capable of recovering to their original shapes; the rate of the recovery was quite dependent on the percentage of POSS termini (or the lengths of PAA chains). For the samples with the higher percentage of POSS (e.g., POSS-PAA2K and POSS-PAA4K), the recovered shapes were indistinguishable from the original shapes, indicating the excellent shape fixity and recovery (Fig. 10). Herewith, we defined the distance (h) from vertex to chord of specimen semicircle (Scheme 1); the recovery (R) can be written as below:

$$R = \frac{h_0 - h_t}{h_0} \times 100\% \tag{3}$$

where h_0 is the initial distance between vortex of specimen semicircle and chord and h_t is that while the specimen have been recovered at time t. Shown in Figure 11 are the plots of R as functions of time (t). For the plain PAA, R always equaled zero, suggesting that this sample did not display the shape memory behavior. In marked contrast to the plain PAA, all the POSS-capped PAA samples displayed the sigmoid

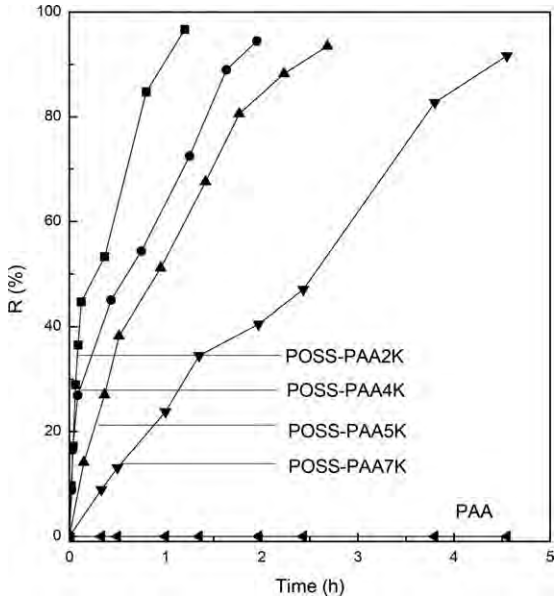

FIGURE 11 Plot of shape recovery (R) as function of time (t) for POSS-capped PAAs at 25 °C.

curve of R versus t, indicating that the shape memory behavior was exhibited. For POSS-PAA2K, the R value attained as high as 90% within 1 h. The rate of recovery increased with increasing the percentage of POSS termini (or decreasing the lengths of PAA chains). This observation indicates that capping POSS to the chain ends significantly promoted the shape memory properties of PAAs.

The shape memory behavior was also investigated by means of DMTA with POSS-PAA2K sample. Shown in Figure 13 are the five one-way shape memory cycles for POSS-PAA2K. The measurement began at 35 °C, at which the specimen was elongated up to 3.2%. Thereafter, the specimen was cooled to −40 °C at the rate of 3 °C min^{-1} to fix the temporal shape; the applied load was then removed. While heated up to 35 °C at the rate of 3 °C min^{-1}, the specimen would

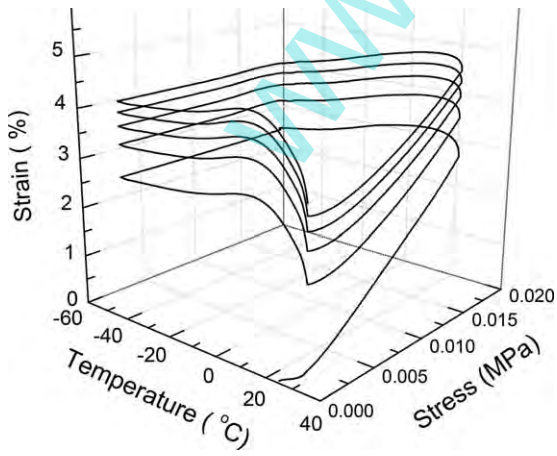

FIGURE 12 DMTA curves for the measurements of one-way shape memory cycles of POSS-PAA2K.

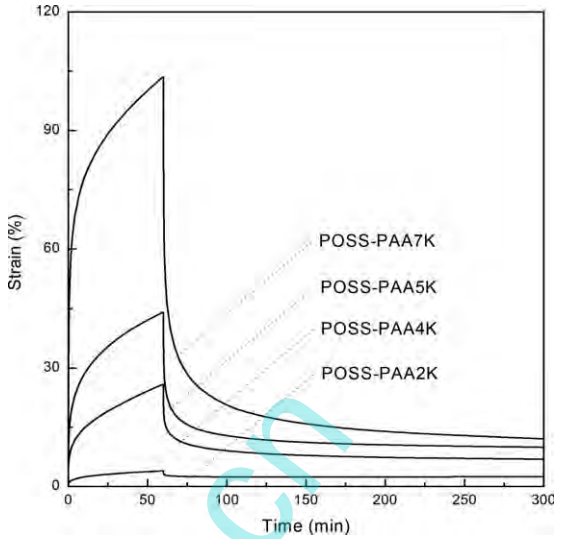

FIGURE 13 Creep curves of POSS-capped PAAs at 25 °C.

recover the original shape due to entropic elasticity. In this work, we repeated the cycle five times. Besides that there was a slight slipping of the specimen from the fixtures during the first cycle, it was observed that the shape memory behavior was quite reproducible, especially while the number of cycle was three or higher. This observation indicates that the sample displayed an excellent shape memory behavior. The shape memory properties are readily accounted for the creep-recovery tests at room temperature. The creep-recovery tests were carried out with the constant stress of $\sigma = 100$ N/m^2 within 1 h and the recovery tests were performed within 6 h. Shown in Figure 3 are the plots of strain as functions of time for the POSS-capped PAAs. It is seen that the values of strain (ε) at $t = 60$ min increased with increasing the lengths of PAA chains. For POSS-PAA2K, the value of strain was $\varepsilon = 3.9\%$, whereas the value of $\varepsilon = 105\%$ was found for POSS-PAA7K at $t = 60$ min. The increased values of strain reflected that the cross-linking densities of the physically cross-linked networks increased with increasing the lengths of PAA chains. In the recovery tests, there were some permanent deformations for all these POSS-capped PAAs. The permanent deformation was decreased with increasing the percentage of POSS. For POSS-PAA2K, the strain at $t = 300$ min was measured to be $\varepsilon = 2.4\%$, whereas the value of strain was measured to be $\varepsilon = 12\%$ for POSS-PAA7K. The creep-recovery tests indicate that capping POSS to the ends of chains significantly promoted the formation of the physically cross-linked networks. In principle, shape memory polymers are a class of elastic polymer networks, the elasticity of which resulted from the change in conformation entropy of the network chains while the cross-linked networks are switched from temporary to permanent shapes with various external stimuli.[60–63] The formation of the cross-linking can be in chemical or physical cross-linking manner. Physical cross-linking is formed with a polymer whose morphology is composed of at least two segregated microdomains as in block copolymers. In the present cases,

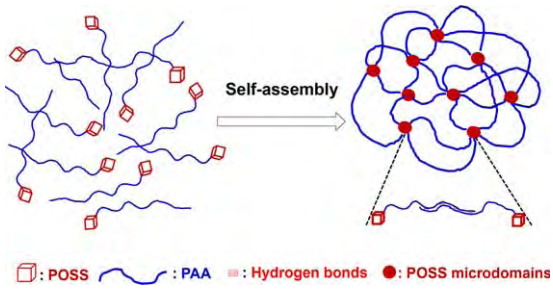

SCHEME 3 The combination of POSS microdomains with the intermolecular hydrogen-bonding interactions results in the formation of stable physical cross-linked networks. [Color figure can be viewed at wileyonlinelibrary.com]

the following three types of intermolecular interactions are responsible for the formation of the physical cross-linking: (i) the macromolecular entanglement; (ii) the intermolecular hydrogen-bonding interactions; and (iii) the formation of POSS microdomains via POSS–POSS interactions. The effect of the macromolecular entanglement could be negligibly small as the molecular weights of PAA were quite low ($M_n < 10{,}000$ Da). In fact, the plain PAA ($M_n = 20{,}000$ Da with $M_w/M_n = 1.1$) cannot even be used for the creep test as it was a viscous fluid at this temperature. In PAA, the intermolecular hydrogen-bonding interactions resulted from the side amide groups of PAA. For plain PAA and the POSS-capped PAAs, there were no significant differences in the density of the hydrogen-bonding interactions. As a class of dynamic bonds, the intermolecular hydrogen-bonding interactions are not sufficient to promote the formation of the stable physically cross-linked networks in the materials. In the POSS-capped PAAs, the POSS microdomains were formed via the POSS–POSS interactions[27,28] as revealed by TEM and SAXS results (Figs. 3 and 4). Nonetheless, the POSS microdomains in the materials were insufficient to promote the formation of physical cross-linking as the POSS cages were only capped to the single ends of PAA chains. It is the combination of the POSS microdomains via the POSS–POSS interactions and the intermolecular hydrogen-bonding interactions that resulted in the formation of the stable physical cross-linked networks (Scheme 12). In other words, both the formation of the POSS microdomains and the self-association of PAA chains constitute the structural basis of shape memory properties.

CONCLUSION

In this work, we successfully synthesized a series of POSS-capped PAAs *via* RAFT polymerization approach. TEM indicates that the POSS-capped PAAs were microphase-separated and the POSS microdomains were formed via the POSS–POSS interactions. In the selective solvents (e.g., methanol), the organic–inorganic hybrids were capable of self-assembling into the spherical nanoobjects. The measurements of static contact angles showed that the surface hydrophobicity of PAA was significantly enhanced with the capping of the POSS groups to the ends of PAA chains. It was found that the formation of the POSS microdomains endowed the organic–inorganic hybrids with typical shape memory properties, which was in marked contrast to the plain PAA with the similar molecular weights. It is proposed that the combination of the POSS–POSS interactions and intermolecular hydrogen-bonding interactions endowed the organic–inorganic semitelechelics with the shape memory properties as evidenced by the creep-recovery tests.

ACKNOWLEDGMENTS

The financial supports from Natural Science Foundation of China (No. 51133003 and 21274091) were gratefully acknowledged. The authors thank the Shanghai Synchrotron Radiation Facility for the support under the projects of Nos. 10sr0260 & 10sr0126.

REFERENCES

1 M. G. Voronkov, V. I. Lavrent'yev, *Top. Curr. Chem.* **1982**, *102*, 199–236.

2 P. D. Lickiss, F. Rataboul, *Adv. Organomet. Chem.* **2008**, *57*, 1–116.

3 J. J. Schwab, J. D. Lichtenhan, *Appl. Organomet. Chem.* **1998**, *12*, 707–713.

4 Y. Abe, T. Gunji, *Prog. Polym. Sci.* **2004**, *29*, 149–182.

5 S. H. Phillips, T. S. Haddad, S. J. Tomczak, *Curr. Opin. Solid State Mater. Sci.* **2004**, *8*, 21–29.

6 R. M. Laine, M. F. Roll, *Macromolecules* **2011**, *44*, 1073–1109.

7 S. W. Kuo, F. C. Chang, *Prog. Polym. Sci.* **2011**, *36*, 1649–1696.

8 K. Y. Pu, B. Zhang, Z. Ma, P. Wang, X. Y. Qi, R. F. Chen, L. H. Wuang, Q. L. Fan, W. Huang, *Polymer* **2006**, *47*, 1970–1978.

9 J. Miyake, Y. Chujo, *Macromol. Rapid Commun.* **2008**, *46*, 8112–8116.

10 S. Bandi, M. Bell, D. A. Schiraldi, *Macromolecules* **2005**, *38*, 9216–9220.

11 J. Mu, S. Zheng, *J. Colloid Interface Sci.* **2007**, *307*, 377–385.

12 K. Zeng, Y. Fang, S. Zheng, *J. Polym. Sci. B Polym. Phys.* **2009**, *47*, 504–516.

13 K. Zeng, L. Wang, S. Zheng, *J. Phys. Chem. B* **2009**, *113*, 11831–11840.

14 M. E. Wright, B. J. Petteys, A. J. Guenthner, S. Fallis, G. R. Yandek, S. J. Tomczak, T. K. Minton, A. Brunsvold, *Macromolecules* **2006**, *39*, 4710–4718.

15 N. Hao, M. Boehning, A. Schoenhals, *Macromolecules* **2007**, *40*, 9672–9679.

16 C. H. Chou, S. L. Hsu, S. W. Yeh, H. S. Wang, K. H. Wei, *Macromolecules* **2005**, *38*, 9117–9123.

17 J. M. Kang, H. J. Cho, J. Lee, J. I. Lee, S. K. Lee, N. S. Cho, D. H. Hwang, H. K. Shi, *Macromolecules* **2006**, *39*, 4999–5008.

18 P. T. Knight, K. M. Lee, T. Chung, P. T. Mather, *Macromolecules* **2009**, *42*, 6596–6605.

19 J. Normatov, M. S. Silverstein, *Macromolecules* **2007**, *40*, 8329–8335.

20 J. Lee, H. J. Cho, B. J. Jung, N. S. Cho, H. K. Shim, *Macromolecules* **2004**, *37*, 8523–8529.

21 C. H. Chou, S. L. Hsu, K. Dinakaran, M. Y. Chiu, K. H. Wei, *Macromolecules* **2005**, *38*, 745–751.

22 W. Lee, S. Ni, J. Deng, B. S. Kim, S. K. Satija, P. T. Mather, A. R. Esker, *Macromolecules* **2007**, *40*, 682–688.

23 H. Yuan, K. Luo, Y. Lai, Y. Pu, B. He, G. Wang, Y. Wu, Z. Gu, *Mol. Pharm.* **2010**, *7*, 953–962.

24 X. Yang, J. D. Froehlich, H. S. Chae, B. T. Harding, S. Li, A. Mochizuki, G. E. Jabbour, *Chem. Mater.* **2010**, *22*, 4776–4782.

25 S. S. Chhatre, J. O. Guardado, B. M. Moore, M. S. Haddad, J. M. Mabry, G. H. McKinley, R. E. Cohen, *ACS Appl. Mater. Interfaces* **2010**, *2*, 3544–3554.

26 B. Decker, C. Hartmann-Thompson, P. I. Carver, S. E. Keinath, P. R. Santurri, *Chem. Mater.* **2010**, *22*, 942–948.

27 L. Matějka, A. Strachota, J. Pleštil, P. Whelan, M. Steinhart, M. Šlouf, *Macromolecules* **2004**, *37*, 9449–9456.

28 A. Strachota, I. Kroutilová, J. Kovářová, L. Matějka, *Macromolecules* **2004**, *37*, 9457–9464.

29 Q. Zhao, H. J. Qi, T. Xie, *Prog. Polym. Sci.* **2015**, *49*, 79–120.

30 L. Sun, W. M. Huang, Z. Ding, Y. Zhao, C. C. Wang, H. Purnawali, C. Tang, *Mater. Des.* **2012**, *33*, 577–640.

31 K. Y. Mya, H. B. Gose, T. Pretsch, M. Bothe, C. He, *J. Mater. Chem.* **2011**, *21*, 4827–4836.

32 M. Bothe, K. Y. Mya, E. M. J. Lin, C. C. Yeo, X. Lu, C. He, T. Pretsch, *Soft Matter* **2012**, *8*, 965–972.

33 K. M. Lee, P. T. Knight, T. Chung, P. T. Mather, *Macromolecules* **2008**, *41*, 4730–4738.

34 B. Alvarado-Tenorio, A. Romo-Uribe, P. T. Mather, *Macromolecules* **2011**, *44*, 5682–5692.

35 B. Alvarado-Tenorio, A. Romo-Uribe, P. T. Mather, *Macromolecules* **2015**, *48*, 5770–5779.

36 I. A. Rousseau, P. T. Mather, *J. Am. Chem. Soc.* **2003**, *125*, 15300–15301.

37 T. Chung, A. Romo-Uribe, P. T. Mather, *Macromolecules* **2008**, *41*, 184–192.

38 J. Wu, Q. Ge, P. T. Mather, *Macromolecules* **2010**, *43*, 7637–7649.

39 C. A. Uraneck, H. L. Hsieh, O. G. Buck, *J. Polym. Sci.* **1960**, *46*, 535–539.

40 R. Jerome, M. Henrioulle-Granville, B. Boutevin, J. Robin, *Prog. Polym. Sci.* **1991**, *16*, 837–906.

41 Y. Tezuka, *Prog. Polym. Sci.* **1992**, *17*, 471–514.

42 Król, P. Linear Polyurethanes: Synthesis Methods, Chemical Structures, Properties and Applications. CRC Press: **2008**.

43 J. Wu, S. Hou, D. Ren, P. T. Mather, *Biomacromolecules* **2009**, *10*, 2686–2693.

44 P. J. Pascault, R. J. J. Williams, In Polymer Blends, Wiley: New York; **2000**; Vol. *1*, pp 379–415.

45 B. S. Kim, P. T. Mather, *Macromolecules* **2002**, *35*, 8378–8384.

46 B. S. Kim, P. T. Mather, *Macromolecules* **2006**, *39*, 9253–9260.

47 B. S. Kim, P. T. Mather, *Polymer* **2006**, *47*, 6202–6207.

48 W. Zhang, A. H. E. Mueller, *Macromolecules* **2010**, *45*, 3148–3152.

49 L. Li, C. Zhang, S. Zheng, *J. Polym. Sci. Part A: Polym. Chem.* **2016**, *DOI: 10.1002/pola.28360*.

50 L. Wang, K. Zeng, S. Zheng, *ACS Appl. Mater. Interfaces* **2011**, *3*, 898–909.

51 Y. Chen, A. M. Kushner, G. A. Williams, Z. Guan, *Nat. Chem.* **2012**, *4*, 467–472.

52 Y. Chen, Z. Guan, *Chem. Commun.* **2014**, *50*, 10868–10870.

53 Y. Chen, Z. Guan, *Polymer* **2015**, *69*, 249–254.

54 R. Wang, C. L. McCormick, A. B. Lowe, *Macromolecules* **2005**, *38*, 9518–9525.

55 K. Koh, S. Sugiyama, T. Morinaga, K. Ohno, Y. Tsujii, T. Fukuda, M. Yamahiro, T. Iijima, H. Oikawa, K. Watanabe, T. Miyashita, *Macromolecules* **2005**, *38*, 1264–1270.

56 D. Kaelble, K. Uy, *J. Adhes.* **1970**, *2*, 66–81.

57 D. Kaelble, Physical Chemistry of Adhesion, Wiley-Interscience: New York, **1971**.

58 A. Adamson, Physical Chemistry of Surfaces, 5th ed.; Wiley Interscience: New York, **1990**.

59 W. S. Rasband, Image J, National Institutes of Health: Bethesda, MD, **2007**. Please see http//rsb.info.nih.gov/ij/index.html, accessed, July **2016**.

60 A. Lendlein, S. Kelch, *Angew. Chem. Int. Ed.* **2002**, *41*, 2034–2057.

61 A. Lendlein, A. M. Schmidt, R. Langer, *Proc. Natl. Acad. Sci.* **2001**, *98*, 842–847.

62 C. Liu, H. Qin, P. T. Mather, *J. Mater. Chem.* **2007**, *17*, 1543–1558.

63 M. Irie, Shape Memory Polymers, Cambridge University Press: Cambridge, **1998**.